CHEMISTRY OF MATERIALS

pubs.acs.org/cm

Article

End-Functionalization of Diarylethene for Opto-Electronic Switching with High Fatigue Resistance

Syed Zahid Hassan,[§] Seong Hoon Yu,[§] Chan So, Dohyun Moon, and Dae Sung Chung*

Cite This: *Chem. Mater.* 2021, 33, 403−412

Read Online

ACCESS | Metrics & More | Article Recommendations | Supporting Information

ABSTRACT: A molecular and synthetic approach to strengthen the switching performance of diarylethene (DAE)-based organic transistors is proposed. By tuning the length of alkyl side chains of the biphenyl unit attached to 1,2-bis(5-biphenyl-2-methylthien-3-yl)perfluorocyclopentene (DAE), we show that the molecular environment for reversible photoisomerization of DAEs can be optimized. Four different DAEs are synthesized with different alkyl chains (DAE_C0, DAE_C1, DAE_C6, and DAE_C10), and ITIC is chosen to construct a semiconductor matrix to maximize the quantum yield of photoconversion considering the complementary absorption range of both materials. From photophysical, structural, and morphological analyses, the longer alkyl chains inhibit intermolecular aggregation between DAEs and allow more hydrophobic surface properties of DAEs, thus improving molecular miscibility with ITIC. The improved molecular compatibility of DAEs with ITIC makes the overall bulk heterojunction film amorphous, allowing more free volume for reversible photoisomerization. Consequently, DAE_C6 exhibits the maximum quantum yield for both photocyclization and photocycloreversion, enabling high light-controlled on/off ratios in photoswitchable transistors. Furthermore, the exceptionally high DAE_C6 quantum yield enables robust fatigue resistance under repeated photoswitching with only a 30% decrease in the on/off ratio after 100 cycles. Overall, this work shows that not only the energy level but also the molecular compatibility can endow significant switching performances for molecular switches.

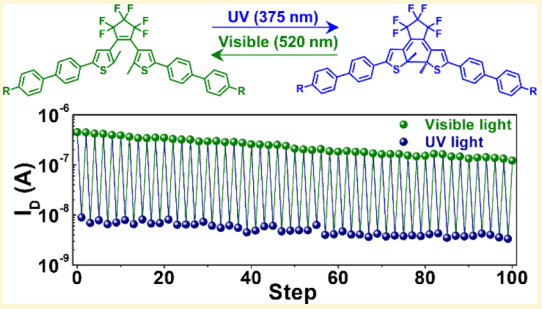

INTRODUCTION

Endowing more and more functionality to the given device dimension can be a smart solution for increasing the integrated circuit density without sacrificing the physical volume of the unit device.[1,2] Embedding a molecular switch in the semiconductor matrix can be a good method to bring such multifunctionality to the unit device, if the selected molecular switch can tune any device electrical properties in a reliable and reproducible way while maintaining the properties of the semiconductor.[3,4] From this point of view, photochromic molecules which use nondestructive light as a stimulus have been vastly applied to various electronic devices, such as field effect transistors (FETs),[5−9] memory devices,[10−13] and bioimaging sensors.[14−16] Photochromic molecules can undergo reversible isomerization in response to light stimuli by producing two interchangeable metastable states. To date, there have been several kinds of photochromic molecules, such as diarylethenes (DAE), azobenzenes, spiropyrans, stilbenes, and fulgides. Among these, DAE is the most promising for embedded molecular switches in thin film devices due to its (1) relatively small volumetric change between two isomers, (2) thermal stability of each metastable state at ambient conditions, and (3) fatigue resistance even after many cycles of light irradiation.[17−20] Photo-induced switching behaviors of thin film organic electronic devices have been reported by several approaches. The most direct approach is the introduction of semiconducting properties to DAEs.[7,21−24] Unfortunately, this approach failed to achieve high performance in terms of both charge carrier mobility and current modulation. Introducing a covalent bond or a supramolecular link between DAEs and the organic semiconductors (OSCs) is another possible approach that can guarantee the maximum areal exposure of DAE to OSCs.[25] However, this approach has the limitation of hampering the molecular arrangement of the semiconductor by changing either the lamellar distance or the $\pi-\pi$ stacking distance. Blending DAEs with OSCs can be the simplest method to not sacrifice the properties of the semiconductor, and very successful demonstrations were introduced by Samorì et al. for many OSCs.[3,4,26−31] In the case of the bulk heterojunction (BHJ) system, the key to the success of electrical switching is how much of the preferred molecular environment can be allowed to each single DAE molecule so that photocyclization and photocycloreversion can be successfully achieved. Therefore, it is important to

Received: October 30, 2020
Revised: December 18, 2020
Published: December 29, 2020

Scheme 1. Synthetic Routes for Biphenyl Substituted DAE Derivatives[a]

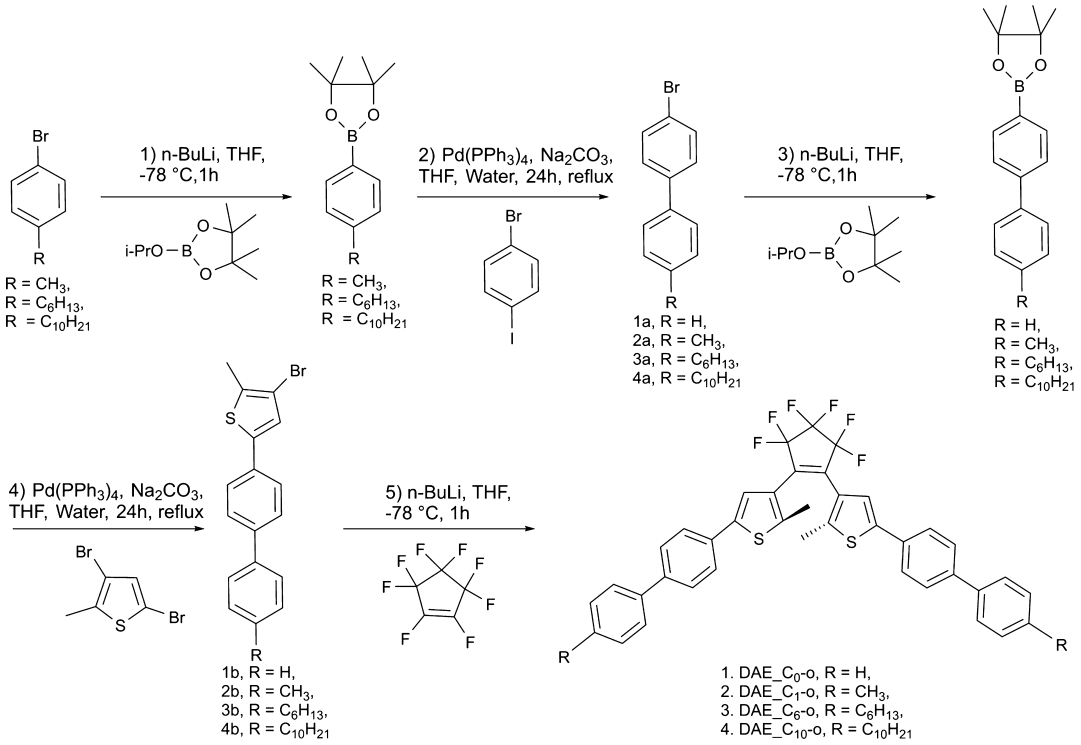

[a](1) *n*-BuLi, tetrahydrofuran (THF), −78 °C, 1 h; 2-isopropoxy-4,4,5,5-tetramethyl-1,3,2-dioxaborolane, −78 °C to rt, 1 h; (2) 1-bromo-4-iodobenzene, $Pd(PPh_3)_4$, Na_2CO_3, reflux; (3) *n*-BuLi, THF, −78 °C, 1 h; 2-isopropoxy-4,4,5,5-tetramethyl-1,3,2-dioxaborolane, −78 °C to rt, 1 h; (4) 3,5-dibromo-2-methylthiophene, $Pd(PPh_3)_4$, Na_2CO_3, reflux; and (5) *n*-BuLi, THF, −78 °C, perfluorocyclopentene, 1 h.

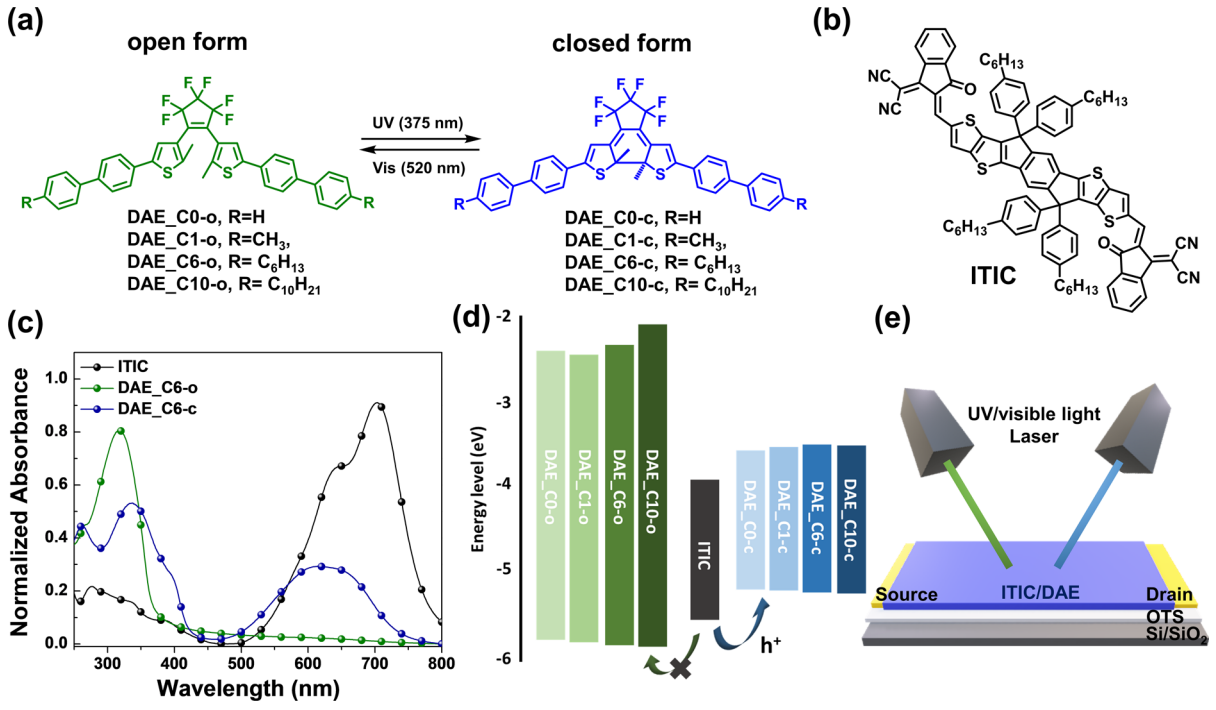

Figure 1. (a) Chemical structures of synthesized biphenyl substituted DAE derivatives, DAE_C0, DAE_C1, DAE_C6, and DAE_C10, in their open- and closed-ring isomers. Reversible photoisomerization of the open-ring isomer to the closed-ring isomer was achieved by irradiating with UV (375 nm) or visible light (520 nm), as displayed in the figure by the arrow, (b) Chemical structure of the OSC, ITIC, (c) UV−visible absorption spectra of ITIC and DAE_C6 in their open- and closed-ring isomers, showing the optical transparency of ITIC in the region of 250−450 nm as compared to the DAE_C6 open-ring isomer, (d) energy level diagram indicating the hole trapping mechanism between the HOMO levels of ITIC and DAE in their open- and closed-ring isomers (energy levels were defined by CV measurements, see Supporting Information), and (e) Device geometry and conceptual image of photoswitching measurements.

https://dx.doi.org/10.1021/acs.chemmater.0c04219
Chem. Mater. 2021, 33, 403−412

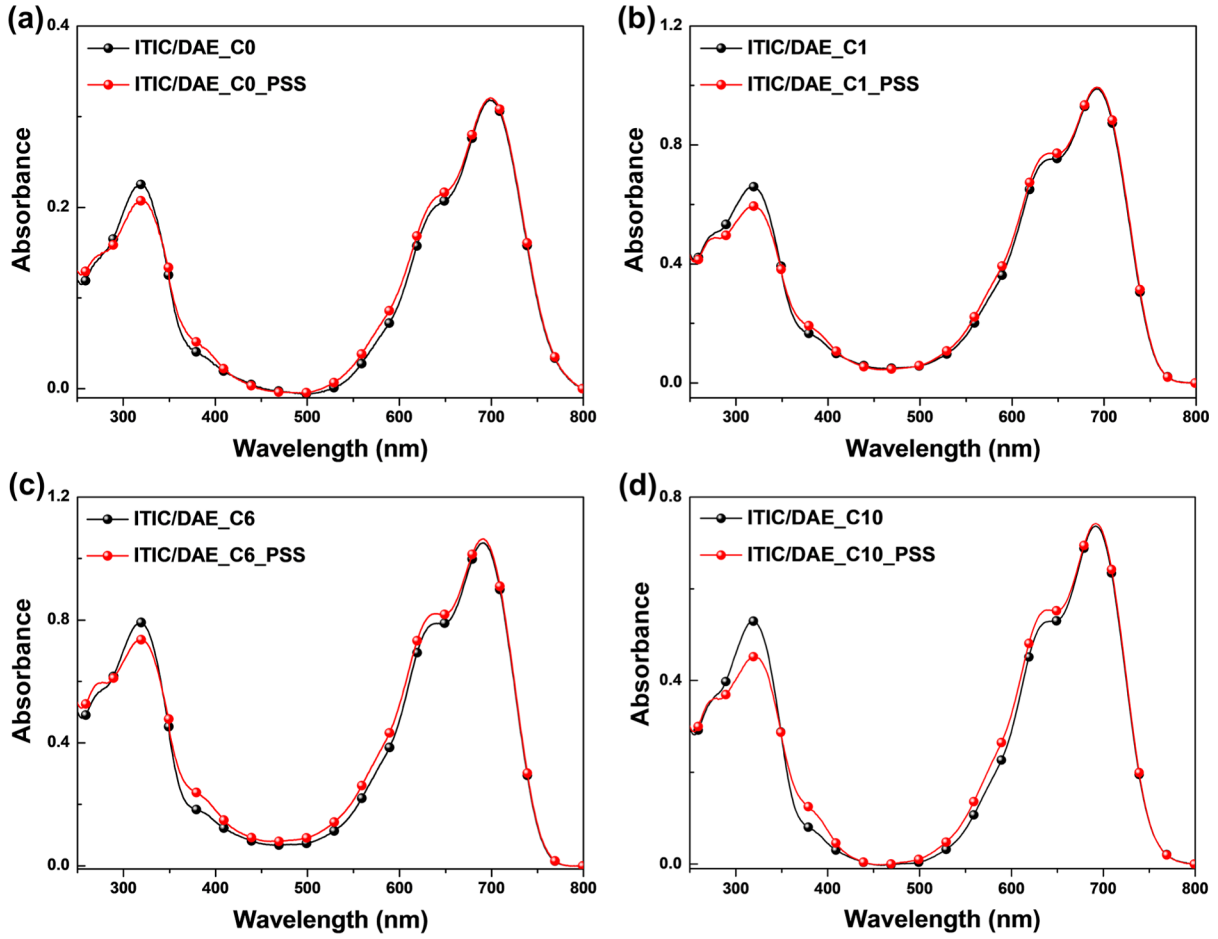

Figure 2. UV−visible absorption spectra of the ITIC/DAE BHJ films and their PSS. (a) ITIC/DAE_C0 BHJ film, (b) ITIC/DAE_C1 BHJ film, (c) ITIC/DAE_C6 BHJ film, and (d) ITIC/DAE_C10 BHJ film. Reversible photoisomerization was carried out by UV light irradiation (375 nm) and visible light irradiation (520 nm). The UV irradiation time was fixed at 3 s and the visible light irradiation time was fixed at 60 s, which showed no further change in the drain current upon further irradiation at the same wavelength.

determine the effects of the DAE molecular structure on the switching performances of the final device.

In this study, to simultaneously maximize the photocyclization/photocycloreversion quantum yield (Q.Y.), and thus the switching performances in FETs, four biphenyl substituted DAE derivatives with different end alkyl chain lengths, namely, DAE_C0, DAE_C1, DAE_C6, and DAE_C10, were systematically designed and synthesized. Concurrently, by varying the alkyl chain, the study attempted to realize an optimal DAE surface energy, which matches that of the π-conjugated OSCs, both of which can be expected to increase photocyclization. Moreover, the study shows that the longer alkyl chains of DAEs can practically reduce the crystalline ordering of the OSCs, allowing more free volume for photocycloreversion. Systematic analyses, to show the morphological/structural effects of DAEs with various alkyl chain lengths, are introduced by means of UV−visible absorption, water contact angle, grazing incidence X-ray diffraction (GIXD), atomic force microscopy (AFM), and differential scanning calorimetry (DSC), followed by detailed discussions.

RESULTS AND DISCUSSION

Synthesis and Characterization. Scheme 1 and Figure 1a summarize the synthetic procedures and chemical structures for DAE_C0, DAE_C1, DAE_C6, and DAE_C10, respectively. A detailed synthetic method for DAE derivatives is presented in the Supporting Information.[7] Biphenyl-substituted DAE, rather than phenyl-substituted DAE, was chosen for the larger π-electron delocalization to achieve a better intermolecular interaction with the OSCs. In fact, DAE with a biphenyl moiety showed semiconductor properties, which is one of the few reported semiconducting DAE derivatives.[7] Perfluorinated DAEs were synthesized because previous works showed that cyclopentene fluorination can make the DAE switching ability faster by a factor of 4−5 with respect to the nonfluorinated analogue.[32−35] 3,9-bis(2-methylene-(3-(1,1-dicyanomethylene)-indanone))-5,5,11,11-tetrakis(4-hexylphenyl)-dithieno[2,3-*d*:2′,3′-d′]-*s*-indaceno[1,2-b:5,6-b′]-dithiophene (ITIC) was chosen as the π-conjugated matrix OSC (Figure 1b),[36−39] because it is a molecular semiconductor and a lower enthalpy of mixing with DAE can be expected when both the molecules have similar surface energies and a higher entropy of mixing with DAE because both of them are small molecules with a molecular weight less than 1500 D. In this case, the change in the Gibbs free energy, $\Delta G = \Delta H - T\Delta S$, can be maximized to a negative value, which can ensure better miscibility between the semiconductor and the molecular switch.[40] Additionally, ITIC was selected as the OSC as it is amorphous until thermally not treated and a suitable candidate for hole trapping as its highest occupied

https://dx.doi.org/10.1021/acs.chemmater.0c04219
Chem. Mater. 2021, 33, 403−412

molecular orbital (HOMO) level is located between the HOMO level of DAE-o and DAE-c. Furthermore, ITIC possesses optical transparency for the absorption range of DAEs synthesized in this study for open isomers (Figure 1c). This implies that a maximized Q.Y. for photocyclization can be expected even though they are blended within the semiconductor matrix. To propose optically switchable transistors using synthesized DAEs, the energy levels of the DAEs were confirmed by cyclic voltammetry (CV). As summarized in Figure 1d and Table S1, the HOMO levels of DAE_C0, DAE_C1, DAE_C6, and DAE_C10 had similar values of ∼−5.8 eV in the open-ring isomer and ∼−5.2 eV in the closed-ring isomer of the synthesized DAEs. Therefore, the increase of the linear alkyl chains at the end of the DAE backbone had a minor effect on the molecular orbitals owing to the minor influence in conjugations; thus, all DAEs showed almost similar optical band gaps. The HOMO levels of these DAEs can induce effective hole carrier trapping by a difference of ∼0.3 eV in the closed form, compared to the HOMO level of ITIC (∼−5.5 eV). In contrast, the open-ring isomer of DAEs has a much deeper HOMO level than that of ITIC and thus does not act as trapping sites for the ITIC hole anymore. Therefore, it can be concluded that DAEs and ITIC can be an effective material combination for photoswitchable optoelectronic devices. Figure 1e schematically depicts the geometric structure of the used ITIC/DAE transistor presenting the bottom gate/bottom source-drain electrode configuration.

Photochemical Studies. To study the photoisomerization behavior of the synthesized series of DAEs, the UV−visible absorption spectra of DAEs in the open-ring isomer, namely, DAE_C0-o, DAE_C1-o, DAE_C6-o, and DAE_C10-o, and the closed-ring isomer, namely, DAE_C0-c, DAE_C1-c, DAE_C6-c, and DAE_C10-c, were obtained in solution, film, and their BHJ film with ITIC. Figure S1 shows the UV−visible absorption spectra of the DAE derivatives in $CHCl_3$ solution. The synthesized DAEs possessed similar absorbance features in both the open-ring and closed-ring isomers as they all have the same π-conjugated structure throughout their molecular backbone. Concurrently, a slight but clear bathochromic shift of both the open- and closed-ring isomers was visible as the alkyl chain length increased, which can be ascribed to the electron donating effect of the longer alkyl chain on the conjugated DAE structure. Figure S2 summarizes the UV−visible absorption spectra of the DAE derivatives in the film state, which shows that photoisomerization is also successful in the film state. To photocyclize DAE-o (open-ring isomer) to DAE-c (closed-ring isomer), the DAE sample was irradiated with UV light (λ = 375 nm) which generated a new absorption band between 450 and 650 nm. Figure 2a−d depicts the UV−visible absorption spectra of the ITIC/DAE BHJ film, before and after UV light irradiation, where the DAE amount in the BHJ film was 40 wt %. Note that a 60%:40% = ITIC/DAE composition by weight was selected in the BHJ film, as it was found that 40 wt % of DAE resulted in the best performance FETs in our studies (Figure S3). Figure S4 depicts the differential changes in the absorption spectra of the ITIC/DAE BHJ film upon UV light irradiation, clearly showing an increase in absorption between 450 and 650 nm and a concomitant decrease in absorption between 275 and 395 nm, indicating the successful conversion of the open-ring isomer to the closed-ring isomer. Overall, the λ_{max} of DAE in the BHJ film was blue-shifted when compared to the pristine DAE film, implying that the DAEs and ITIC were well intermixed (Table 1). Upon continuous irradiation with UV light, the absorption band at λ_{max} for the closed form continuously increased, leading to the generation of a photostationary state (PSS) which is defined as the equilibrium between DAE-o and DAE-c. Photocycloreversion was conducted by irradiating the DAE sample in the PSS with visible light (λ = 520 nm). Note that a green laser with a wavelength of 520 nm was chosen instead of longer wavelength light sources as the ITIC band I absorption sharply increases after ∼550 nm. The absorption maxima for the open- and closed-ring isomers and the PSS and Q.Y. for photocyclization and photocycloreversion of DAE in the BHJ film are listed in Table 1. The detailed methods used for the estimation of PSS and Q.Y. are described in the Supporting Information, which followed methods detailed in previous studies.[41−45] Table S2 summarizes the photoconversion ratio and Q.Y. of DAE_C0, DAE_C1, DAE_C6, and DAE_C10 in the solution and thin film and Table 1 summarizes those in the BHJ films with ITIC. The photoconversion ratio in the solution state exceeded 80% for all the synthesized DAEs, which is caused by rapid conformational changes in the parallel and antiparallel forms of the DAE-o derivatives in solution state at room temperature, as reported earlier.[42] Conformational change of the parallel and antiparallel form of DAEs is not possible in the thin film state. That is, only the photoactive antiparallel form of DAE photocyclizes to the closed-ring isomer and thus the PSS in the thin film is lower than that in the solution state. As summarized in Table 1, both the PSS and Φ_{UV} of DAEs in the BHJ film increased as the length of the alkyl chain increased, presumably because of the bulkier alkyl chain, which can (1) reduce the intermolecular $\pi-\pi$ interaction between DAEs and thus induce more free volume for conformational change and (2) increase the molar portion of the photoactive antiparallel conformer, as DAEs with a bulky alkyl chain length prefer the antiparallel conformer.[46] The exception observed for DAE_C10 had the lowest photocyclization and photocycloreversion Q.Y. which can be ascribed to a very large alkyl chain volume, which requires a very high volumetric change for photoisomerization.[4] Interestingly, the Q.Y. for photocycloreversion also increased as the alkyl chain length was increased. This can be related to volumetric expansion during photocycloreversion. Because a larger DAE volume can ensure a larger space in the open-ring

Table 1. Absorption Characteristics and Photoreactivity of DAEs in the ITIC Matrix

	λ_{max}				
	[a]open form	[b]closed form	[c]conversion ratio (%)	[d]ϕ_{UV}	[e]ϕ_{vis}
ITIC/DAE_C0 film	316	599	48	0.42	0.50
ITIC/DAE_C1 film	316	587	47	0.41	0.51
ITIC/DAE_C6 film	319	599	58	0.68	0.53
ITIC/DAE_C10 film	316	590	53	0.37	0.38

[a]Absorption maxima for the open-ring isomer. [b]Absorption maxima for the closed-ring isomer. [c]Amount of the closed-ring isomer in PSS upon UV light irradiation (375 nm, 0.15 mW/cm^2). [d]Q.Y. of the open- to closed-ring isomer with an experimental error of 10%. [e]Q.Y. of the closed- to open-ring isomer with an experimental error of 10%.

https://dx.doi.org/10.1021/acs.chemmater.0c04219
Chem. Mater. 2021, 33, 403−412

isomer, and as the ITIC matrix becomes amorphous when mixed with DAE, as discussed in the GIXD section, it provides a flexible inner space for the closed-ring isomer to easily recover back to its open-ring isomer form. For example, DAE_C6 showed almost twice the difference in unit cell volume between the two photoisomers, as confirmed by single crystal XRD (Table S3). The relatively high DAE_C6 Q.Y. is also very important for electrical fatigue resistance because a high Q.Y. minimizes the cumulative portion of the undesired conformational isomer.

Studies on Molecular Compatibility. To further elucidate the origin of the highest photocyclization and photocycloreversion Q.Y. of DAE_C6, the molecular compatibility of the synthesized DAEs with ITIC was studied by means of surface energy, GIXD, AFM, and DSC analyses. To investigate the effect of different alkyl chains on the surface free energy of DAEs, the water contact angle for each pristine ITIC, DAEs, and their BHJ films was measured. Because DAEs were dissolved in diiodomethane, the calculation of the surface free energy could not be completed. In the case of the pristine ITIC film, the average water contact angle was 95.6 ± 0.7°, and there was a slight change in the contact angle after exposure to UV light, which also highlights the photostability of ITIC along with the negligible change observed in the UV−visible absorption spectrum of ITIC before and after UV light irradiation, as shown in Figure S5. In the case of the pristine DAE films, the overall hydrophobicity was enhanced when the DAE molecules photoisomerized from open- to closed-ring isomers by UV exposure, such that the water contact angle for DAE_C0 changed from 79.5 ± 1.1 to 91.3 ± 1.0°, DAE_C1 changed from 79.8 ± 0.6 to 93.3 ± 1.0°, DAE_C6 changed from 92.4 ± 0.7 to 101.0 ± 0.9°, and DAE_C10 changed from 91.4 ± 0.3 to 98.1 ± 0.5° (Figure S6).[47,48] This phenomenon is due to the denser intermolecular packing of DAE molecules in the closed form, as the overall cell volume decreased when the DAE open-ring isomer changed to the closed-ring isomer, as studied by single crystal XRD (Figure S7a−d and Table S3).[49] Additionally, as the DAE alkyl chain length was increased, the DAE thin film became more hydrophobic leading to a higher water contact angle. Because the DAEs and their BHJ solutions with ITIC were kept in dark conditions, it can be assumed that most DAEs remain as open-ring isomers when their solutions were deposited onto the substrate for spin coating. Therefore, a similar hydrophobicity of the open-ring isomer is needed for better miscibility with ITIC. The difference in the water contact angle of DAE_C0, DAE_C1, DAE_C6, and DAE_C10 with the ITIC was approximately 16.1 ± 1.1, 15.8 ± 0.7, 3.2 ± 0.7, and 4.1 ± 0.7°, respectively. This implies that the miscibility of ITIC/DAE_C0 and ITIC/DAE_C1 was poorer than ITIC/DAE_C6 and ITIC/DAE_C10.[50] In this context, DAE_C6 with a water contact angle of 92.4 ± 0.7° should have minimized the surface free energy difference with ITIC, which has a water contact angle of ~95.6 ± 0.7°. This explains the optimized miscibility of DAE_C6 within the ITIC matrix, allowing the hydrophobic alkyl chains of DAE_C6 to be exposed to the surface more efficiently, which explains the higher hydrophobicity of the ITIC/DAE_C6 BHJ film as compared to the pristine ITIC film. Interestingly, the ITIC/DAE_C10 BHJ film showed a slightly lower or similar water contact angle to that of the ITIC/DAE_C6 BHJ film, as shown in Figure 3, which could be caused by the random molecular packing of DAE_C10 because of very long alkyl chains.[51] Therefore, it was concluded that DAE_C6 can be an optimal counterpart to ITIC by means of molecular compatibility. In a similar context, we can also explain the lowest switching performance in the case of DAE_C0.

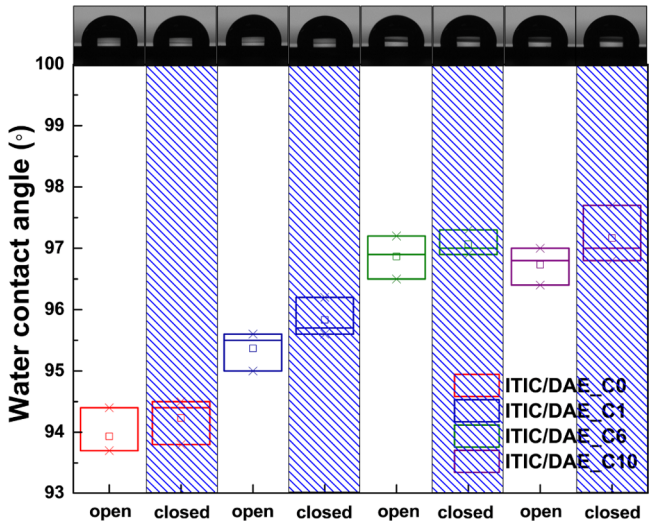

Figure 3. Water contact angle of ITIC/DAE_C0, ITIC/DAE_C1, ITIC/DAE_C6, and ITIC/DAE_C10 BHJ films, where DAE is in both open- and closed-ring isomer forms. Photoisomerization of the open-ring isomer to the closed-ring isomer was achieved by irradiating the samples with UV light. The boxes in the plot represent the standard deviation of the measured water contact angle. The water contact angle values were obtained from five independent points at room temperature. The actual water droplets on the ITIC/DAE BHJ film surface are shown in the upper part of the figure.

Two-dimensional GIXD analyses were performed to examine the crystalline ordering changes of the ITIC/DAE BHJ films when the DAE alkyl chain length was changed.[52,53] Note that post thermal annealing was not employed for all the ITIC/DAE BHJ films. Figure 4a−f shows the GIXD pattern images, as well as out-of-plane line cut profiles of the ITIC and ITIC/DAE BHJ films.[36,54] In-plane line cut profiles of the ITIC/DAE BHJ films are summarized in Figure S8a. The pristine ITIC film shows weak diffraction features with a small diffraction peak at q_z = 0.42 Å^{-1} (100) because no thermal treatment was used. When mixed with DAEs, the ITIC/DAE BHJ films exhibited considerably less featured diffraction patterns. Overall, the ITIC lamellar diffraction peak (100) gradually broadened as the DAE alkyl chain length increased. The lamellar spacing increased to 15.93 and 16.46 Å in the ITIC/DAE_C0 and the ITIC/DAE_C1 BHJ films, respectively, as compared to the ITIC lamellar spacing of 14.65 Å, which suggest that DAE molecules intercalated within the ITIC crystalline domains. The lamellar spacing for ITIC/DAE_C6 and ITIC/DAE_C10 could not be obtained as the GIXD patterns became completely featureless. Additionally, the $\pi-\pi$ spacing for ITIC/DAEs could not be obtained because of very weak diffraction in that region (Table S4). This was somewhat expected because the DAEs studied herein are not crystalline as they are simply cast on the substrate (Figure S8b−d). However, it forms a crystalline packing when assembled as a single crystal in the solution, as shown by the single crystal structure (Figure S7). Clearly, it can be concluded that the overall crystalline ordering of the ITIC/DAE BHJ film worsened as the alkyl chain length of the synthesized DAEs increased. Additionally, we could obtain

https://dx.doi.org/10.1021/acs.chemmater.0c04219
Chem. Mater. 2021, 33, 403−412

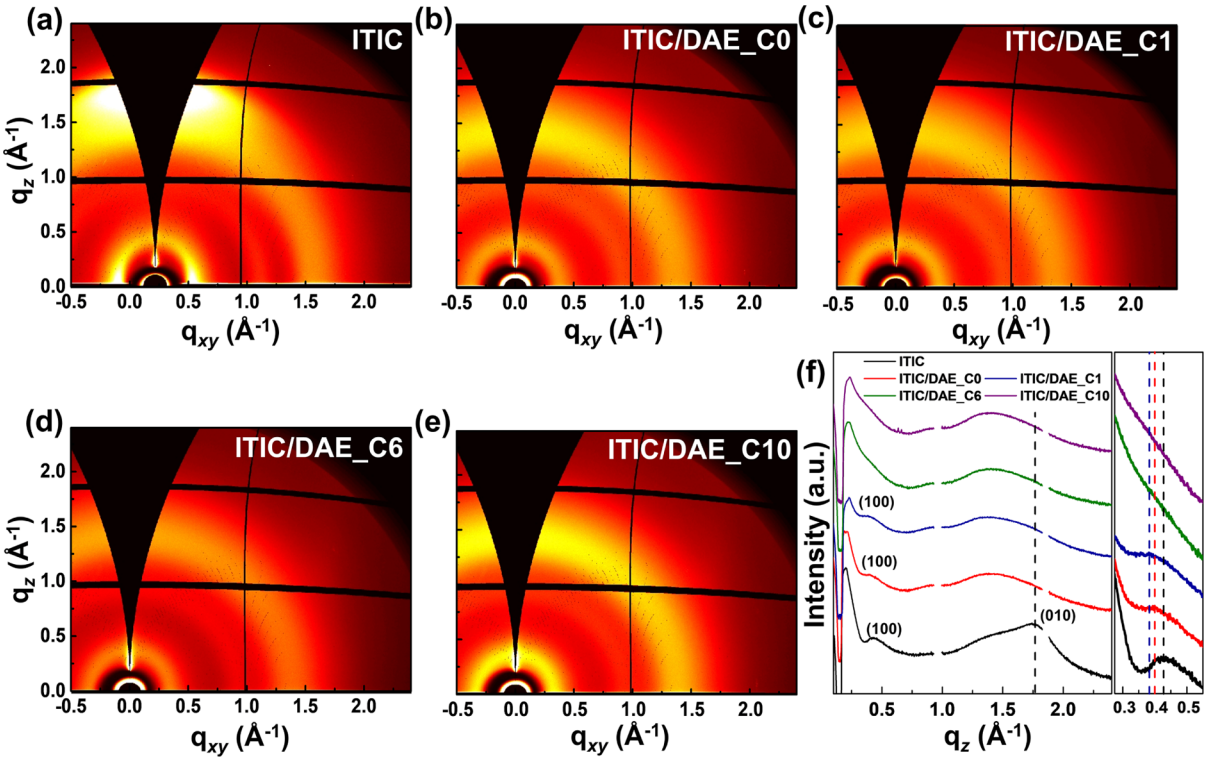

Figure 4. Two-dimensional GIXD images of (a) ITIC, (b) ITIC/DAE_C0 BHJ film, (c) ITIC/DAE_C1 BHJ film, (d) ITIC/DAE_C6 BHJ film, (e) ITIC/DAE_C10 BHJ film, and (f) corresponding line cut profiles in the out-of-plane direction where the right side of the line cut profile shows a magnification between 0.3 and 0.5 $Å^{-1}$ and where the dashed line shows the shift in the (100) peak in the ITIC/DAE BHJ films when the alkyl chain length was increased (black dashed line = ITIC, red dashed line = ITIC/DAE_C0, and blue dashed line = ITIC/DAE_C1).

only negligible change in in-plane or out-of-plane line cut profile for ITIC/DAE BHJ films upon UV exposure which suggest that the films remain mostly amorphous regardless of photoisomerization (Figure S9).

Moreover, the melting point obtained from DSC showed a slightly lower melting point in the case of the ITIC/DAE_C6 BHJ as compared to the pristine ITIC, as shown in Figure S10a,b, which also implies that the ITIC was well mixed with DAE_C6.[3,55,56] Additionally, the morphological differences between the ITIC/DAE_C6 BHJ film and the pristine ITIC were also investigated by means of AFM, as summarized in Figure S11. The pristine ITIC exhibited a granular morphology, a feature of small crystalline domains, while all the different weight ratio (10, 20, 40, and 60 wt %) samples of the ITIC/DAE_C6 BHJ films exhibited a featureless morphology with considerably lower root mean square (rms) roughness. The roughness of the ITIC/DAE_C6 BHJ films decreased as compared to the pristine ITIC film from ∼0.55 to ∼0.25 nm as the DAE content increased. Interestingly, the rms roughness value was also the lowest in the case of the 40 wt % ITIC/DAE_C6 BHJ film (Figure S12), implying the optimized miscibility between ITIC and DAE_C6. Additionally, the change in surface morphology before and after UV exposure was investigated; however, the phase separation phenomenon could not be found in either condition.

Switching Performance. To elucidate the switching behavior of the synthesized DAEs, bottom gate/bottom contact FETs were fabricated for all the ITIC/DAE BHJ films. ITIC exhibits a typical ambipolar behavior as shown in Figure S13a,b. In this study, the p-type nature of ITIC was utilized to induce the hole trapping mechanism by the DAE molecules. Figure S14 shows that there was no change in the n-type behavior of the ITIC/DAE_C6 FET performance after UV and visible light irradiation, which is obvious as the lowest unoccupied molecular orbital (LUMO) levels of both the open- and closed-ring isomers of DAE are shallower than that of ITIC. The switching performance of all the FETs is defined by the following equation

$$\text{ON/OFF ratio} = |I_{VIS}|/|I_{UV}|$$

where I_{VIS} is the initial drain current or after visible light irradiation and I_{UV} is the drain current after UV light irradiation from the I_{DS} versus V_G plot where V_{DS} and V_G was fixed to −20 and −30 V, respectively. Figure S3 shows the switching performance of the ITIC/DAE_C6 FETs when 10, 20, 40, and 60 wt % DAE_C6 were added. The ITIC/DAE_C6 FET with 40 wt % of DAE showed the best switching performance in terms of drain current. All the DAEs enabled a successful current modulation between the on/off states with an on/off ratio exceeding 20; however, the degree of current modulation between the on/off states became highest in the case of ITIC/DAE_C6 with the maximum on/off ratio of 50, consistent with the observation of the maximum Φ_{UV} and Φ_{vis}. Additionally, we have calculated the hole mobilities for ITIC/DAE_C0, ITIC/DAE_C1, ITIC/DAE_C6, and ITIC/DAE_C10 OFETs in their open and closed form as summarized in Table S5.[57,58] From the threshold voltage of the transfer curve, the trap density can be estimated using the following equation

$$N_{tr} = \frac{C_i V_{th}}{e}$$

where C_i is the capacitance of a dielectric layer, V_{th} is the threshold voltage extracted from transfer characteristics, and e

https://dx.doi.org/10.1021/acs.chemmater.0c04219
Chem. Mater. 2021, 33, 403−412

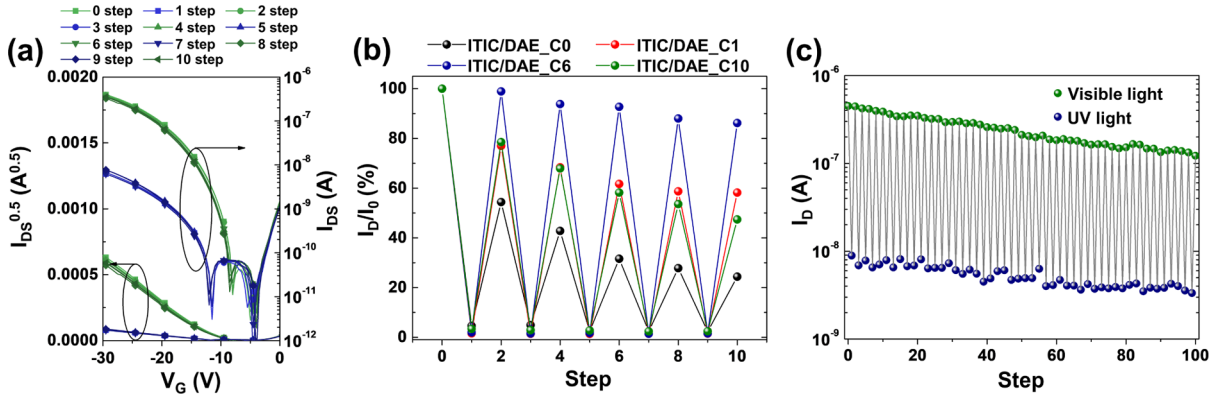

Figure 5. Photoswitching performance of ITIC/DAE FET devices. (a) Transfer curves of the ITIC/DAE_C6-based FETs for alternate steps of UV (375 nm) and visible (520 nm) light irradiation up to 10 cycles. (b) Continuous switching behavior of the ITIC/DAEs based FETs after irradiation with UV (375 nm, 0.15 mW/cm^2) and visible light (520 nm, 0.15 mW/cm^2) of up to 10 cycles. The connecting lines are used as guides. Each current value was extracted from the transfer curves repeated up to 10 cycles. (c) Reversible modulation of the drain current of the ITIC/DAE_C6 based FETs irradiated with UV (375 nm, 0.15 mW/cm^2) and visible light (520 nm, 0.15 mW/cm^2) up to 100 cycles. The UV irradiation time was fixed at 3 s, and the visible light irradiation time was fixed at 60 s, with no further change in the drain current being observed upon further irradiation at the same wavelength. All single points of the I_D values were extracted from the transfer curves at $V_G = -30$ V and $V_{DS} = -20$ V. The enlarged figure of switching behavior in the ITIC/DAEs based FETs under UV (375 nm) irradiation extracted from Figure 5b can be found in Figure S15 for better readability.

is the electron charge. Because of photoisomerization, ITIC/DAE_C6 FETs showed an increase in the concentration of trap states from ~1.45 × 10^{12} to ~2.27 × 10^{12} cm^{-2} for pristine and UV exposure condition, respectively (Table S6).[57]

The electrical fatigue resistance of the best performing ITIC/DAE_C6 FET was determined, and it showed only a 10% decrease in the drain current after 10 on/off repetitive steps, while all other ITIC/DAE FETs exhibited considerably worse fatigue resistance, which again corresponds to the observation of the maximum DAE_C6 Φ_{UV} and Φ_{vis} (Figures 5a−c and S16a−c). Furthermore, the ITIC/DAE_C6 FET could maintain a reasonably good on/off ratio exceeding 35, even after a continuous switching operation of 100 cycles, which is a decrease of ~30% from the initial on/off ratio. The comparison in the photoswitching performance of our FET devices with recently reported works with various molecular switches is summarized in Table S7.

Theoretically, the ITIC/DAE FET electrical fatigue resistance is dependent on not only the molecular photostability of DAE against bi-product generation but also the Q.Y. for photocyclization/photocycloreversion. This is because, in the case of low Q.Y., the cumulative proportion of isomers whose conformation has not adequately changed is continuously increased under continuous photoswitching. Therefore, the success of DAE_C6 for electrical fatigue resistance can be attributed to its rather high Q.Y. for both photocyclization and photocycloreversion as compared to all other previously reported DAEs.[4,7,21,26]

As summarized in the photophysics section, the conversion ratio and both the Φ_{UV} and the Φ_{vis} increased as the DAE alkyl length was increased. The increasing conversion ratio and Φ_{UV} of the DAEs with longer alkyl chains in the BHJ films with ITIC can be explained by the decreased intermolecular interaction between the DAE molecules due to steric hindrance of the bulky alkyl chain and also by the decreased surface energy difference between DAE and ITIC. Additionally, as suggested in the structural/morphological analyses section, the increasing Φ_{vis} of the DAEs with longer alkyl chains can be attributed to a more amorphous ordering of ITIC within the BHJ films with the presence of bulkier DAE molecules, which allows more free volume for photocycloreversion. Because of such synergistic advantages of DAE_C6, we believe that a very successful photo-controlled electrical switching behavior in FETs could be achieved. Electrical fatigue resistance up to 100 repetitive cycles of programmed UV−visible exposure has never been demonstrated with any kind of molecular switches.

CONCLUSIONS

This study attempted to secure a strategic molecular approach to maximize the switching behavior of DAEs when mixed with organic π-conjugated semiconductors. Biphenyl substituted DAE derivatives with different alkyl chain lengths were successfully designed and synthesized and were employed as ITIC FET photoswitches. Systematic photophysical, surface energy, structural, and morphological analyses demonstrated that (1) longer alkyl chain DAEs can be helpful in deriving better miscibility with ITIC due to the suppressed intermolecular interaction between the DAEs and the more similar surface characteristics and (2) longer alkyl chain DAEs can allow more free volume for conformational change of themselves by more efficiently inhibiting the crystalline ordering of ITIC. Thanks to these synergistic effects of DAE_C6, a high on/off ratio exceeding 50 and an exceptional electrical fatigue resistance, up to 100 repetitive cycles, were demonstrated. We believe that this work can be a milestone highlighting the importance of molecular compatibility between the molecular switch and the semiconductor to maximize the photoswitching performances.

EXPERIMENTAL SECTION

Single Crystal Studies. To know the molecular conformation and photoreactivity in crystal state of the newly synthesized DAE, X-ray crystallographic analysis was carried out.[59] DAE_C6 was deliberately selected for crystal studies as it showed highest miscibility with ITIC and better FET performance. Plate-shaped DAE_C6-o crystals were obtained by recrystallization from chloroform and acetonitrile mixture. Figure S7a shows the crystal structure of an open-ring isomer. The distance between reactive carbon was found to

https://dx.doi.org/10.1021/acs.chemmater.0c04219
Chem. Mater. 2021, 33, 403−412

be 3.6 Å which is suitable for photocyclization as reported earlier.[60−63] For yielding a closed-ring isomer in crystal state, the mounted DAE_C6-o sample was irradiated with UV light, but there was no change in the crystal structure; this could be due to the strong $\pi-\pi$ interaction in the biphenyl ring of DAE_C6 which makes it difficult for reactive carbon and thienyl sulfur to detort their positions to generate the closed-ring isomer. Thus, to obtain the crystal structure in the closed form, the DAE_C6-o solution in chloroform and acetonitrile mixture was continuously irradiated with UV light overnight. Interestingly, a needle-type DAE_C6-c crystal was obtained. The obtained crystal structure for the closed-ring isomer is shown in Figure S7b, in which the distance between reactive carbon was only 1.5 Å which suggests that DAE_C6 is crystallized in the closed form. Crystallographic data obtained for the abovementioned crystals are shown in Table S3. Molecular packing for open- and closed-ring isomers is shown in Figure S7c,d, respectively. The crystal data files of DAE_C6-o and DAE_C6-c were deposited into the Cambridge Crystallographic Data Centre (CCDC) and assigned numbers 2038757 and 2038758, respectively (Supporting Information).

Device Fabrication. Highly n-doped Si++/SiO_2 (100 nm) wafers were used as substrates and gate. The FET geometry is a bottom contact/bottom gate with a W/L ratio of 1580 (channel length = 5 μm). The interdigitated Ti/Au source and drain electrodes are prepatterned on the substrates. The prepatterned substrates were cleaned sequentially with a detergent (Mucasol), deionized water, acetone, and 2-propanol by sonication and dried with nitrogen flow. Dried substrates were treated with a UV−ozone cleaner to remove various contaminants on the surface. Then, the substrates were immersed in a mixture of OTS (0.3 mL) and toluene (60 mL) for 30 min, followed by annealing at 120 °C for 1 h. The OTS-treated substrates were rinsed with toluene and dried with nitrogen flow. The solution of ITIC/DAEs was spin coated on the OTS-treated prepatterned substrates at 2000 rpm for 1 min.

Measurements. ^{1}H NMR and ^{13}C NMR spectra were recorded with a Bruker ADVANCE-400 spectrometer which operated at 400 MHz for ^{1}H nuclei, 100 MHz for ^{13}C nuclei, and 376.5 MHz for ^{19}F nuclei and are internally referenced to residual solvent signals. Chemical shifts are reported in parts per million (ppm). Differential scanning calorimetry (DSC) was conducted under nitrogen on a TA Instrument (PerkinElmer DSC 4000). The sample was heated at 10 °C/min from 30 to 300 °C. UV−vis absorption spectra were measured by UV 1650PC spectrophotometer.

To analyze the surface of the films, contact angle measurements and AFM (Park Systems, XE-150) were conducted. The PLS-II 2D and 3C beamlines at the Pohang Accelerator Laboratory (PAL) in Korea was used for confirmation of the crystalline profiles. All the films were manufactured in the same manner as that of the FETs were fabricated. CV was conducted using an IviumStat instrument and conducted at a scan rate of 50 mV s^{-1} at room temperature under nitrogen, with 0.1 M tetrabutylammonium hexafluorophosphate in acetonitrile as the electrolyte; each compound was deposited onto the working electrode from a chloroform solution. All CV measurements were carried out with a conventional three-electrode configuration employing a glassy carbon electrode as the working electrode, saturated calomel electrode as the reference electrode, and Pt wire as the counter electrode. The electrical characteristics of the FETs were measured using a parameter analyzer (Keithley 4200A) in a nitrogen-filled glovebox at room temperature. To observe the optical switching behavior, a laser with a wavelength of 375 nm for the on state and a laser with a wavelength of 520 nm for the off state were set up inside the nitrogen-filled glovebox. Charge carrier mobilities were calculated using the equation $\Delta I_{DS} = (WC_i\mu/2L) \times (V_{GS} - V_{th})^2$, where I_{DS} is the source-drain current, C_i is the capacitance per unit area of the dielectric layer, μ represents mobility, W and L are the channel width and length, and V_{GS} and V_{th} are the gate voltage and the threshold voltage, respectively.[57,58]

■ ASSOCIATED CONTENT

Supporting Information

The Supporting Information is available free of charge at https://pubs.acs.org/doi/10.1021/acs.chemmater.0c04219.

Synthesis and characterization details, Q.Y. estimation method, X-ray crystallography, OFET data, surface analysis, GIXD, DSC, and AFM (PDF)

Crystallographic information for DAE_C6-o and DAE_C6-c (ZIP)

■ AUTHOR INFORMATION

Corresponding Author

Dae Sung Chung − *Department of Chemical Engineering, Pohang University of Science & Technology (POSTECH), Pohang 37673, Republic of Korea;* orcid.org/0000-0003-1313-8298; Email: dchung@postech.ac.kr

Authors

Syed Zahid Hassan − *Department of Chemical Engineering, Pohang University of Science & Technology (POSTECH), Pohang 37673, Republic of Korea*

Seong Hoon Yu − *Department of Chemical Engineering, Pohang University of Science & Technology (POSTECH), Pohang 37673, Republic of Korea*

Chan So − *Department of Chemical Engineering, Pohang University of Science & Technology (POSTECH), Pohang 37673, Republic of Korea*

Dohyun Moon − *Department of Beamline, Pohang Accelerator Laboratory, Pohang 37673, Republic of Korea;* orcid.org/0000-0002-6903-0270

Complete contact information is available at: https://pubs.acs.org/10.1021/acs.chemmater.0c04219

Author Contributions

[§]S.Z.H. and S.H.Y. contributed equally to this work.

Notes

The authors declare no competing financial interest.

■ ACKNOWLEDGMENTS

This work was supported by the National Research Foundation of Korea (NRF) grant funded by the Korea government (MSIT) (No. 2020R1A4A1019455 and No. 2020M3F3A2A03082631).

■ ABBREVIATIONS

DAE, diarylethene; ITIC, 3,9-bis(2-methylene-(3-(1,1-dicyanomethylene)-indanone))-5,5,11,11-tetrakis(4-hexylphenyl)-dithieno[2,3-*d*:2′,3′-*d*′]-*s*-indaceno[1,2-*b*:5,6-*b*′]dithiophene; GIXD, grazing incidence X-ray diffraction; FET, field-effect transistor; OSC, organic semiconductor; Q.Y., quantum yield; DSC, differential scanning calorimetry; NMR, nuclear magnetic resonance; HOMO, the highest occupied molecular orbital; LUMO, the lowest unoccupied molecular orbital

■ REFERENCES

(1) Gelinck, G.; Heremans, P.; Nomoto, K.; Anthopoulos, T. D. Organic Transistors in Optical Displays and Microelectronic Applications. *Adv. Mater.* **2010**, *22*, 3778−3798.

(2) Muccini, M. A bright future for organic field-effect transistors. *Nat. Mater.* **2006**, *5*, 605−613.

(3) El Gemayel, M.; Börjesson, K.; Herder, M.; Duong, D. T.; Hutchison, J. A.; Ruzié, C.; Schweicher, G.; Salleo, A.; Geerts, Y.;

Hecht, S.; Orgiu, E.; Samorì, P. Optically switchable transistors by simple incorporation of photochromic systems into small-molecule semiconducting matrices. *Nat. Commun.* **2015**, *6*, 6330.
(4) Hou, L.; Leydecker, T.; Zhang, X.; Rekab, W.; Herder, M.; Cendra, C.; Hecht, S.; McCulloch, I.; Salleo, A.; Orgiu, E.; Samorì, P. Engineering Optically Switchable Transistors with Improved Performance by Controlling Interactions of Diarylethenes in Polymer Matrices. *J. Am. Chem. Soc.* **2020**, *142*, 11050−11059.
(5) Shen, Q.; Wang, L.; Liu, S.; Cao, Y.; Gan, L.; Guo, X.; Steigerwald, M. L.; Shuai, Z.; Liu, Z.; Nuckolls, C. Photoactive Gate Dielectrics. *Adv. Mater.* **2010**, *22*, 3282−3287.
(6) Tian, J.; Fu, L.; Liu, Z.; Geng, H.; Sun, Y.; Lin, G.; Zhang, X.; Zhang, G.; Zhang, D. Optically Tunable Field Effect Transistors with Conjugated Polymer Entailing Azobenzene Groups in the Side Chains. *Adv. Funct. Mater.* **2019**, *29*, 1807176.
(7) Hayakawa, R.; Higashiguchi, K.; Matsuda, K.; Chikyow, T.; Wakayama, Y. Optically and Electrically Driven Organic Thin Film Transistors with Diarylethene Photochromic Channel Layers. *ACS Appl. Mater. Interfaces* **2013**, *5*, 3625−3630.
(8) Zhang, H.; Hui, J.; Chen, H.; Chen, J.; Xu, W.; Shuai, Z.; Zhu, D.; Guo, X. Synergistic Photomodulation of Capacitive Coupling and Charge Separation Toward Functional Organic Field-Effect Transistors with High Responsivity. *Adv. Electron. Mater.* **2015**, *1*, 1500159.
(9) Hou, L.; Zhang, X.; Cotella, G. F.; Carnicella, G.; Herder, M.; Schmidt, B. M.; Pätzel, M.; Hecht, S.; Cacialli, F.; Samorì, P. Optically switchable organic light-emitting transistors. *Nat. Nanotechnol.* **2019**, *14*, 347−353.
(10) Frolova, L. A.; Troshin, P. A.; Susarova, D. K.; Kulikov, A. V.; Sanina, N. A.; Aldoshin, S. M. Photoswitchable organic field-effect transistors and memory elements comprising an interfacial photochromic layer. *Chem. Commun.* **2015**, *51*, 6130−6132.
(11) Zhang, C.; Zhou, H.-P.; Liao, L.-Y.; Feng, W.; Sun, W.; Li, Z.-X.; Xu, C.-H.; Fang, C.-J.; Sun, L.-D.; Zhang, Y.-W.; Yan, C.-H. Luminescence Modulation of Ordered Upconversion Nanopatterns by a Photochromic Diarylethene: Rewritable Optical Storage with Nondestructive Readout. *Adv. Mater.* **2010**, *22*, 633−637.
(12) Zheng, K.; Han, S.; Zeng, X.; Wu, Y.; Song, S.; Zhang, H.; Liu, X. Rewritable Optical Memory Through High-Registry Orthogonal Upconversion. *Adv. Mater.* **2018**, *30*, 1801726.
(13) Dashitsyrenova, D. D.; Lvov, A. G.; Frolova, L. A.; Kulikov, A. V.; Dremova, N. N.; Shirinian, V. Z.; Aldoshin, S. M.; Krayushkin, M. M.; Troshin, P. A. Molecular structure−electrical performance relationship for OFET-based memory elements comprising unsymmetrical photochromic diarylethenes. *J. Mater. Chem. C* **2019**, *7*, 6889−6894.
(14) Li, C.; Xiong, K.; Chen, Y.; Fan, C.; Wang, Y.-L.; Ye, H.; Zhu, M.-Q. Visible-Light-Driven Photoswitching of Aggregated-Induced Emission-Active Diarylethenes for Super-Resolution Imaging. *ACS Appl. Mater. Interfaces* **2020**, *12*, 27651−27662.
(15) Zhang, Z.; Zhang, J.; Wu, B.; Li, X.; Chen, Y.; Huang, J.; Zhu, L.; Tian, H. Diarylethenes with a Narrow Singlet−Triplet Energy Gap Sensitizer: a Simple Strategy for Efficient Visible-Light Photochromism. *Adv. Opt. Mater.* **2018**, *6*, 1700847.
(16) Naren, G.; Hsu, C.-W.; Li, S.; Morimoto, M.; Tang, S.; Hernando, J.; Guirado, G.; Irie, M.; Raymo, F. M.; Sundén, H.; Andréasson, J. An all-photonic full color RGB system based on molecular photoswitches. *Nat. Commun.* **2019**, *10*, 3996.
(17) Goulet-Hanssens, A.; Eisenreich, F.; Hecht, S. Enlightening Materials with Photoswitches. *Adv. Mater.* **2020**, *32*, 1905966.
(18) Zhang, J.; Zou, Q.; Tian, H. Photochromic Materials: More Than Meets The Eye. *Adv. Mater.* **2013**, *25*, 378−399.
(19) Irie, M.; Fukaminato, T.; Matsuda, K.; Kobatake, S. Photochromism of Diarylethene Molecules and Crystals: Memories, Switches, and Actuators. *Chem. Rev.* **2014**, *114*, 12174−12277.
(20) Irie, M. Diarylethenes for Memories and Switches. *Chem. Rev.* **2000**, *100*, 1685−1716.
(21) Kurokawa, Y.; Hayakawa, R.; Shimada, S.; Tanaka, K.; Higashiguchi, K.; Noguchi, Y.; Matsuda, K.; Wakayama, Y. Photocontrollable ambipolar transistors with π-conjugated diarylethene photochromic channels. *Jpn. J. Appl. Phys.* **2019**, *58*, SDDH03.
(22) Tsuruoka, T.; Hayakawa, R.; Kobashi, K.; Higashiguchi, K.; Matsuda, K.; Wakayama, Y. Laser Patterning of Optically Reconfigurable Transistor Channels in a Photochromic Diarylethene Layer. *Nano Lett.* **2016**, *16*, 7474−7480.
(23) Hayakawa, R.; Petit, M.; Higashiguchi, K.; Matsuda, K.; Chikyow, T.; Wakayama, Y. Interface engineering for improving optical switching in a diarylethene-channel transistor. *Org. Electron.* **2015**, *21*, 149−154.
(24) Kurokawa, Y.; Hayakawa, R.; Shimada, S.; Higashiguchi, K.; Noguchi, Y.; Matsuda, K.; Wakayama, Y. Ambipolar carrier transport in an optically controllable diarylethene thin film transistor. *Org. Electron.* **2019**, *64*, 205−208.
(25) Kim, E.; Lee, H. W. Photo-induced electrical switching through a mainchain polymer. *J. Mater. Chem.* **2006**, *16*, 1384−1389.
(26) Carroli, M.; Duong, D. T.; Buchaca-Domingo, E.; Liscio, A.; Börjesson, K.; Herder, M.; Palermo, V.; Hecht, S.; Stingelin, N.; Salleo, A.; Orgiu, E.; Samorì, P. The Role of Morphology in Optically Switchable Transistors Based on a Photochromic Molecule/p-Type Polymer Semiconductor Blend. *Adv. Funct. Mater.* **2020**, *30*, 1907507.
(27) Orgiu, E.; Crivillers, N.; Herder, M.; Grubert, L.; Pätzel, M.; Frisch, J.; Pavlica, E.; Duong, D. T.; Bratina, G.; Salleo, A.; Koch, N.; Hecht, S.; Samorì, P. Optically switchable transistor via energy-level phototuning in a bicomponent organic semiconductor. *Nat. Chem.* **2012**, *4*, 675−679.
(28) Rekab, W.; Leydecker, T.; Hou, L.; Chen, H.; Kirkus, M.; Cendra, C.; Herder, M.; Hecht, S.; Salleo, A.; McCulloch, I.; Orgiu, E.; Samorì, P. Phototuning Selectively Hole and Electron Transport in Optically Switchable Ambipolar Transistors. *Adv. Funct. Mater.* **2020**, *30*, 1908944.
(29) Li, Y.; Zhang, H.; Qi, C.; Guo, X. Light-driven photochromism-induced reversible switching in P3HT−spiropyran hybrid transistors. *J. Mater. Chem.* **2012**, *22*, 4261−4265.
(30) Zhang, H.; Guo, X.; Hui, J.; Hu, S.; Xu, W.; Zhu, D. Interface Engineering of Semiconductor/Dielectric Heterojunctions toward Functional Organic Thin-Film Transistors. *Nano Lett.* **2011**, *11*, 4939−4946.
(31) Börjesson, K.; Herder, M.; Grubert, L.; Duong, D. T.; Salleo, A.; Hecht, S.; Orgiu, E.; Samorì, P. Optically switchable transistors comprising a hybrid photochromic molecule/n-type organic active layer. *J. Mater. Chem. C* **2015**, *3*, 4156−4161.
(32) Hania, P. R.; Pugzlys, A.; Lucas, L. N.; de Jong, J. J. D.; Feringa, B. L.; van Esch, J. H.; Jonkman, H. T.; Duppen, K. Ring Closure Dynamics of BTE-Based Photochromic Switches: Perfluoro- versus Perhydrocyclopentene Derivatives. *J. Phys. Chem. A* **2005**, *109*, 9437−9442.
(33) Herder, M.; Schmidt, B. M.; Grubert, L.; Pätzel, M.; Schwarz, J.; Hecht, S. Improving the Fatigue Resistance of Diarylethene Switches. *J. Am. Chem. Soc.* **2015**, *137*, 2738−2747.
(34) Qiu, H.; Liu, Z.; Yao, Y.; Herder, M.; Hecht, S.; Samorì, P. Simultaneous Optical Tuning of Hole and Electron Transport in Ambipolar WSe2 Interfaced with a Bicomponent Photochromic Layer: From High-Mobility Transistors to Flexible Multilevel Memories. *Adv. Mater.* **2020**, *32*, 1907903.
(35) Staykov, A.; Yoshizawa, K. Photochemical Reversibility of Ring-Closing and Ring-Opening Reactions in Diarylperfluorocyclopentenes. *J. Phys. Chem. C* **2009**, *113*, 3826−3834.
(36) Xie, D.; Liu, T.; Gao, W.; Zhong, C.; Huo, L.; Luo, Z.; Wu, K.; Xiong, W.; Liu, F.; Sun, Y.; Yang, C. A Novel Thiophene-Fused Ending Group Enabling an Excellent Small Molecule Acceptor for High-Performance Fullerene-Free Polymer Solar Cells with 11.8% Efficiency. *Sol. RRL* **2017**, *1*, 1700044.
(37) Yang, F.; Li, C.; Lai, W.; Zhang, A.; Huang, H.; Li, W. Halogenated conjugated molecules for ambipolar field-effect transistors and non-fullerene organic solar cells. *Mater. Chem. Front.* **2017**, *1*, 1389−1395.
(38) Hoang, M. H.; Park, G. E.; Choi, S.; Park, C. G.; Park, S. H.; Nguyen, T. V.; Kim, S.; Kwak, K.; Cho, M. J.; Choi, D. H. High-

efficiency non-fullerene polymer solar cell fabricated by a simple process using new conjugated terpolymers. *J. Mater. Chem. C* **2019**, *7*, 111−118.
(39) Park, Y.; Fuentes-Hernandez, C.; Jia, X.; Larrain, F. A.; Zhang, J.; Marder, S. R.; Kippelen, B. Measurements of the field-effect electron mobility of the acceptor ITIC. *Org. Electron.* **2018**, *58*, 290−293.
(40) Blanks, R. F. Thermodynamics of Polymer Solutions. *Polym. Plast. Technol. Eng.* **1977**, *8*, 13−33.
(41) Stranius, K.; Börjesson, K. Determining the Photoisomerization Quantum Yield of Photoswitchable Molecules in Solution and in the Solid State. *Sci. Rep.* **2017**, *7*, 41145.
(42) Santos, A. R.; Ballardini, R.; Belser, P.; Gandolfi, M. T.; Iyer, V. M.; Moggi, L. Photochemical investigation of a photochromic diarylethene compound that can be used as a wide range actinometer. *Photochem. Photobiol. Sci.* **2009**, *8*, 1734−1742.
(43) Pariani, G.; Bianco, A.; Castagna, R.; Bertarelli, C. Kinetics of Photochromic Conversion at the Solid State: Quantum Yield of Dithienylethene-Based Films. *J. Phys. Chem. A* **2011**, *115*, 12184−12193.
(44) Han, Y.; Spangler, L. H. Use of Isosbestic Points for Determination of Quantum Efficiency in Transient Absorption Spectroscopy. *J. Phys. Chem. A* **2002**, *106*, 1701−1707.
(45) Yamaguchi, T.; Irie, M. Photochromism of bis(2-alkyl-1-benzothiophen-3-yl)perfluorocyclopentene derivatives. *J. Photochem. Photobiol., A* **2006**, *178*, 162−169.
(46) Kingo, U.; Eriko, T.; Yoshifumi, A.; Shinichiro, N.; Masahiro, I. Substitution Effect on the Coloration Quantum Yield of a Photochromic Bisbenzothienylethene. *Chem. Lett.* **1999**, *28*, 63−64.
(47) Nishimura, R.; Hyodo, K.; Mayama, H.; Yokojima, S.; Nakamura, S.; Uchida, K. Dual wettability on diarylethene microcrystalline surface mimicking a termite wing. *Commun. Chem.* **2019**, *2*, 90.
(48) Uchida, K.; Izumi, N.; Sukata, S.; Kojima, Y.; Nakamura, S.; Irie, M. Photoinduced Reversible Formation of Microfibrils on a Photochromic Diarylethene Microcrystalline Surface. *Angew. Chem., Int. Ed.* **2006**, *45*, 6470−6473.
(49) Kobatake, S.; Takami, S.; Muto, H.; Ishikawa, T.; Irie, M. Rapid and reversible shape changes of molecular crystals on photoirradiation. *Nature* **2007**, *446*, 778−781.
(50) Zhang, L.; Xing, X.; Zheng, L.; Chen, Z.; Xiao, L.; Qu, B.; Gong, Q. Vertical phase separation in bulk heterojunction solar cells formed by in situ polymerization of fulleride. *Sci. Rep.* **2014**, *4*, 5071.
(51) Lu, F.; Takaya, T.; Iwata, K.; Kawamura, I.; Saeki, A.; Ishii, M.; Nagura, K.; Nakanishi, T. A Guide to Design Functional Molecular Liquids with Tailorable Properties using Pyrene-Fluorescence as a Probe. *Sci. Rep.* **2017**, *7*, 3416.
(52) Rivnay, J.; Mannsfeld, S. C. B.; Miller, C. E.; Salleo, A.; Toney, M. F. Quantitative Determination of Organic Semiconductor Microstructure from the Molecular to Device Scale. *Chem. Rev.* **2012**, *112*, 5488−5519.
(53) Baker, J. L.; Jimison, L. H.; Mannsfeld, S.; Volkman, S.; Yin, S.; Subramanian, V.; Salleo, A.; Alivisatos, A. P.; Toney, M. F. Quantification of Thin Film Crystallographic Orientation Using X-ray Diffraction with an Area Detector. *Langmuir* **2010**, *26*, 9146−9151.
(54) Li, W.; Li, G.; Guo, X.; Guo, B.; Bi, Z.; Guo, H.; Ma, W.; Ou, X.; Zhang, M.; Li, Y. Efficient non-fullerene polymer solar cells based on a wide bandgap polymer of meta-alkoxy-phenyl-substituted benzodithiophene and difluorobenzotriazole. *J. Mater. Chem. A* **2017**, *5*, 19680−19686.
(55) Yi, N.; Ai, Q.; Zhou, W.; Huang, L.; Zhang, L.; Xing, Z.; Li, X.; Zeng, J.; Chen, Y. Miscibility Matching and Bimolecular Crystallization Affording High-Performance Ternary Nonfullerene Solar Cells. *Chem. Mater.* **2019**, *31*, 10211−10224.
(56) Lv, R.; Chen, D.; Liao, X.; Chen, L.; Chen, Y. A Terminally Tetrafluorinated Nonfullerene Acceptor for Well-Performing Alloy Ternary Solar Cells. *Adv. Funct. Mater.* **2019**, *29*, 1805872.
(57) Podzorov, V.; Menard, E.; Borissov, A.; Kiryukhin, V.; Rogers, J. A.; Gershenson, M. E. Intrinsic Charge Transport on the Surface of Organic Semiconductors. *Phys. Rev. Lett.* **2004**, *93*, 086602.
(58) McCulloch, I.; Salleo, A.; Chabinyc, M. Avoid the kinks when measuring mobility. *Science* **2016**, *352*, 1521−1522.
(59) Ishida, S.; Kitagawa, D.; Kobatake, S.; Kim, S.; Kurihara, S.; Fukaminato, T. Efficient "turn-off" fluorescence photoswitching in a highly fluorescent diarylethene single crystal. *Chem. Commun.* **2019**, *55*, 5681−5684.
(60) Kobatake, S.; Hasegawa, H.; Miyamura, K. High-Convertible Photochromism of a Diarylethene Single Crystal Accompanying the Crystal Shape Deformation. *Cryst. Growth Des.* **2011**, *11*, 1223−1229.
(61) Morimoto, M.; Kobatake, S.; Irie, M. Crystal engineering of photochromic diarylethene single crystals. *Chem. Rec.* **2004**, *4*, 23−38.
(62) Morimoto, M.; Irie, M. Photochromism of diarylethene single crystals: crystal structures and photochromic performance. *Chem. Commun.* **2005**, *31*, 3895−3905.
(63) Irie, M.; Kobatake, S.; Horichi, M. Reversible Surface Morphology Changes of a Photochromic Diarylethene Single Crystal by Photoirradiation. *Science* **2001**, *291*, 1769−1772.

https://dx.doi.org/10.1021/acs.chemmater.0c04219
Chem. Mater. 2021, 33, 403−412